

RSC Advances



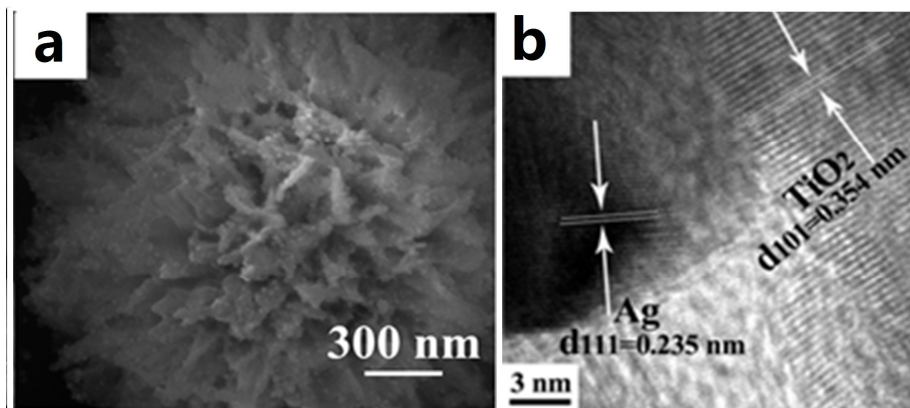
This is an *Accepted Manuscript*, which has been through the Royal Society of Chemistry peer review process and has been accepted for publication.

Accepted Manuscripts are published online shortly after acceptance, before technical editing, formatting and proof reading. Using this free service, authors can make their results available to the community, in citable form, before we publish the edited article. This *Accepted Manuscript* will be replaced by the edited, formatted and paginated article as soon as this is available.

You can find more information about *Accepted Manuscripts* in the [Information for Authors](#).

Please note that technical editing may introduce minor changes to the text and/or graphics, which may alter content. The journal's standard [Terms & Conditions](#) and the [Ethical guidelines](#) still apply. In no event shall the Royal Society of Chemistry be held responsible for any errors or omissions in this *Accepted Manuscript* or any consequences arising from the use of any information it contains.

Graphical Contents Entry



Novel flower-shaped microspheres (FSMP) TiO₂/Ag Nanoparticles composites were fabricated by the facile tyrosine-reduced method and used as a photocatalyst for the degradation of MB under light irradiation. The results indicate that as-prepared composite microspheres have a superior photocatalytic activity attributed to higher surface area, increased light absorption capability, the reduction of electron-hole pair recombination.

A Facile Synthesis of Flower-Shaped TiO₂/Ag microspheres and Application in Photocatalyst

Li Zhang^{1,*}, Lei Chen², Liangwei Chen¹, and Guang Zhu^{1,*}

⁵ Received (in XXX, XXX) Xth XXXXXXXXX 200X, Accepted Xth XXXXXXXXX 200X

First published on the web Xth XXXXXXXXX 200X

DOI: 10.1039/b000000x

Flower-shaped microspheres (FSMPs) TiO₂ were successfully prepared using a sol-hydrothermal technique. A facile tyrosine-reduced method was adopted to reduce the Ag precursor to Ag nanoparticles (NPs) on surface of as-prepared TiO₂ FSMPs. The morphology, structure and photocatalytic activity in the degradation of methylene blue (MB) of TiO₂/Ag FSMPs were characterized by scanning electron microscopy, transmission electron microscopy, X-ray diffraction, UV-vis absorption spectroscopy, Raman spectroscopy and X-ray photoelectron spectroscopy, respectively. The results show that the photocatalytic activity of TiO₂/Ag FSMPs is superior to that of TiO₂ FSMPs and P25, which is attributed to the unique flower-shaped morphology with high surface area, the increased light absorption, and the reduction of photoelectron-hole pair recombination in TiO₂ with the introduction of Ag NPs.

1. Introduction

TiO₂ is one of the most promising materials for solar energy conversion due to its appropriate band gap, strong oxidizing ability, long-term stability against photocorrosion and chemical corrosion, low cost and facile preparation.¹⁻⁵ It has been widely investigated recently as a useful material in the treatment of wastewater and polluted air. However, the high recombination rate (around 90%) of photon-induced electron and hole pairs limits the photocatalytic activities of TiO₂.^{6, 7} Recently, some researches show that the composite of TiO₂ and metal nanomaterials with a work function lower than the conduction band of TiO₂, such as Ag, Au, or Fe, can solve the problem and enhance the photocatalytic activity of TiO₂ in the UV or visible light region.⁸⁻¹⁴ In the photocatalysis process, these metal nanomaterials can act as excellent electron-acceptor/transport materials to effectively facilitate the migration of photo-induced electrons and hinder the charge recombination in electron-transfer processes due to the electronic interaction between TiO₂ and them, which enhances the photocatalytic performance.¹⁵⁻¹⁸

Among the various noble metals, nanosized Ag exhibits high surface area to volume ratio, high surface energy with surface defects, unusual electric and optical properties.^{19, 20} Critically, the work function of silver is much lower than that of other noble metals such as gold and platinum, which favors formation of good band alignment.²¹ Therefore, various methods have been developed to prepare TiO₂/Ag composite for photocatalysis. Recently, Zhang et al.²² reported a novel strategy to prepare Ag cluster-doped TiO₂ nanoparticles without addition of any chemical reducing agent and/or organic additive, and the photocatalytic activity was markedly increased via doping Ag nanomaterials for pentachlorophenol degradation. Lu et al.²³ reported that the Ag/ZnO nanocomposites were prepared by a one-step hydrothermal method for photocatalytic degradation of organic dye pollutants. The results indicated that the as-prepared Ag/ZnO nanocomposites exhibited a higher photocatalytic performance than pure ZnO. Even though, the research of Ag

nanoparticles (NPs) deposited on the novel flower-shaped microspheres (FSMPs) TiO₂ is very limited for photocatalysis.

Herein, we demonstrated that a simple approach to synthesize TiO₂/Ag FSMPs. The porous TiO₂ FSMPs were synthesized by a facile sol-hydrothermal method, and then Ag NPs were deposited on TiO₂ FSMPs via the tyrosine-reduced method. The photocatalytic activities of as-prepared TiO₂/Ag FSMPs in the degradation of methylene blue (MB) were investigated.

2. Experimental details

2.1 Reagents and Materials

Silver nitrate (AgNO₃), sodium hydroxide (NaOH), potassium hydroxide (KOH), hydrochloric acid (HCl), and hydrogen peroxide (H₂O₂) were purchased from Sinopharm Chemical Co. Ltd (Shanghai, China). Titanium powder (Ti) and L-Tyrosine (C₉H₁₁NO₃) were of guarantee reagent (GR) and were purchased from Aldrich. All the chemical reagents were of analytical grade and were used as received without further purification. A Milli-Q water purification system was used to produce water with an average resistivity of 18.25 M·cm for all experiments.

2.2 Synthesis of TiO₂ FSMPs

The porous TiO₂ FSMPs were prepared by a facile sol-hydrothermal method.²⁴ Typically, Ti powder (50 mg) was dissolved in NaOH (70 mL, 10 M) solution under vigorously magnetic stirring for 30 min. Subsequently, H₂O₂ (30%, 0.5 mL) was added into the mixture under stirring. After sonication of 10 min, the mixture was injected into a 100 mL Teflon-lined autoclave and sealed to heat at 180 °C for 1 h, and then allowed to cool to room temperature naturally. The obtained precipitates were centrifuged, washed several times using hydrochloric acid (5%) and distilled water. As-prepared production was dried at

60 °C for 8 h. Finally, porous TiO₂ FSMPs were obtained by calcining at 550 °C for 2 h.

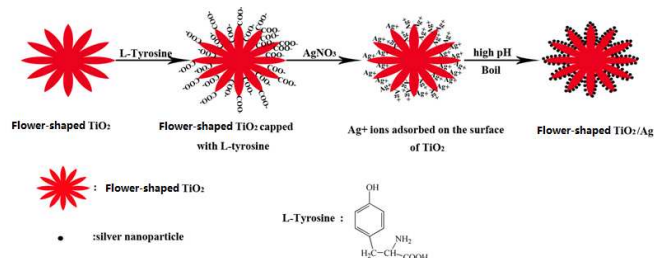


Fig. 1 Schematic formation process of the flower-shaped TiO₂/Ag FSMPs.

2.3 Synthesis of TiO₂/Ag FSMPs

Ag NP was prepared by reducing silver nitrate (AgNO₃) under alkaline conditions,²⁵ and deposited on the surface of as-prepared porous TiO₂ FSMPs (as shown in Fig. 1). In briefly, 30 mg of as-prepared porous TiO₂ FSMPs was completely dispersed into 30 mL aqueous solution under vigorously magnetic stirring for 30 min. The TiO₂ aqueous solution was injected into 100 mL three-neck round-bottom flask and preheated under magnetic stirring in an oil bath heated to 35 °C. After 10 min, 10 ml of L-Tyrosine solution as catalyst was added to three-neck round-bottom flask under magnetic stirring for 30 min. Subsequently, the mixture were heated to 90 °C to remove superfluous L-Tyrosine, and 10 mL of 10⁻³ M AgNO₃ and 1 mL of 10⁻¹ M KOH solution were added into the mixture under stirring at 90 °C, respectively. The mixture solution was allowed to heat until its color changed from white to black. The obtained samples were centrifuged, and washed several times by using distilled water, which indicates that the pH of sample solution is ca 7. At last, the samples were dried in a vacuum at 60 °C overnight, and collected for further characterization.

2.4 Characterization

The UV-Visible absorption spectrum was measured by a Shimadzu UV-2550 spectrometer. The morphology and structure of as-prepared samples were characterized by an FEI Sirion 200 field-emission scanning electronic microscopy (FESEM; Eindhoven, The Netherlands), high resolution transmission electron microscopy (HRTEM JEOL 2010) and X-ray diffraction (XRD, Japan MAC Science Co.), respectively. Raman spectra were carried out on a LabRAM HR800 confocal microscope Raman system (Horiba Jobin Yvon) with 532 and 633 nm excitation sources. X-ray photoelectron spectroscopy (XPS) measurements were carried out on an ESCALAB 250 X-ray photoelectron spectrometer (American Thermo Co.), at a pressure greater than 10⁻⁶ Pa. Brunauer-Emmett-Teller (BET) surface area was measured by ASAP 2020 Accelerated Surface Area and Porosimetry System (Micrometitics, Norcross, GA).

2.5 Photocatalytic degradation of MB

The photocatalytic activities of TiO₂/Ag FSMPs were evaluated via decomposing MB at room temperature. The concentration of MB and photocatalyst were set as 20 mg/L and 1 g/L, respectively. Prior to irradiation, the suspensions were magnetically stirred in the dark for 30 min to establish an adsorption/desorption equilibrium. The dispersions were kept under constant air-equilibrated conditions before and during irradiation. The photocatalytic degradation process was observed by the change of the absorbance maximum in optical absorption spectra of MB dye. The aqueous dispersions of TiO₂/Ag FSMPs were typically prepared by addition of 60 mg of TiO₂/Ag FSMPs to a 60 mL aqueous solution containing 1 × 10⁻⁵ M MB dye. A 350 W Xe lamp without cutoff filter was employed as a irradiation source with wavelength from ultraviolet to visible, and located 20 cm away from the reactor to trigger the photocatalytic reaction. A certain volume of suspension were drawn at selected times for analysis. The absorbance spectra of the temporal variations of the MB dye were recorded by a Shimadzu UV-3310 spectrometer. In the meantime, as-prepared TiO₂ FSMPs and commercial P25 (Degussa, BET area 50 m²/g; particle size, 20-30 nm) were also tested under identical conditions for comparison.

3. Results and discussion

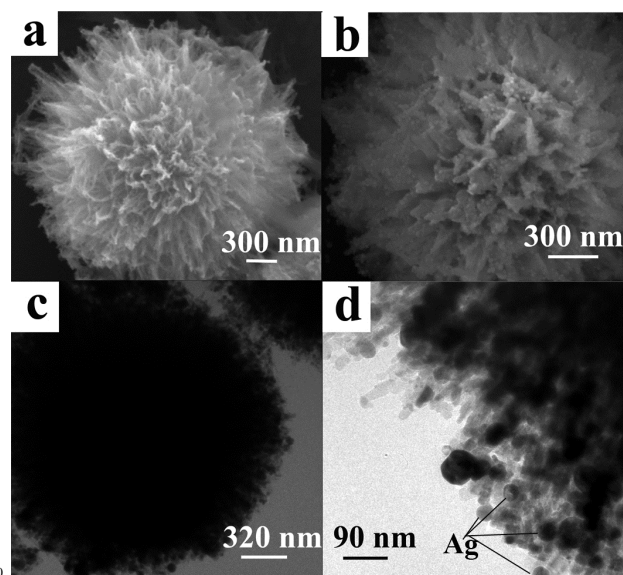


Fig. 2 (a) and (b) FESEM images of as-prepared TiO₂ and TiO₂/Ag FSMPs, and (c) and (d) HRTEM images of as-prepared TiO₂/Ag FSMPs.

Fig. 2a and 2b show FESEM images of as-prepared TiO₂ and TiO₂/Ag FSMPs. It can be observed that TiO₂ are composed of self-assembled radial nano-flakes with a larger surface area, and TiO₂ display three-dimensional FSMPs hierarchical morphology with the size of about 2 ± 0.2 μm. A lot of nanoparticles can be observed on the surface of TiO₂ FSMPs after loading Ag NPs. Fig. 2c and d show HRTEM images of TiO₂/Ag FSMPs. The as-prepared Ag NPs with the average diameter of 30 nm are deposited randomly on the surface of

TiO₂ FSMPs, forming the strong interaction between the Ag NPs and TiO₂ FSMPs.

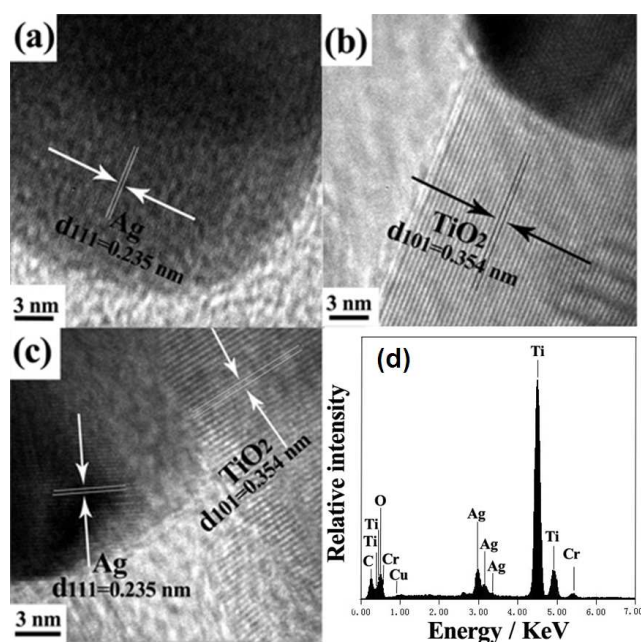


Fig. 3 HRTEM images of the as-prepared TiO₂/Ag FSMPs, and EDS spectrum corresponding to sample shown in HRTEM image.

Fig. 3 shows HRTEM images of as-prepared TiO₂/Ag FSMPs. It can be found that the estimated interplanar spacings of Ag NPs and flower-like hierarchical morphology TiO₂ are 0.235 and 0.354 nm based on the (111) and (101) lattice plane of cubic Ag and anatase TiO₂, respectively.^{26,27} As shown in Figure 3c, it can be also seen that Ag NPs can be attached onto the surface of TiO₂, leading to a good contact between Ag and TiO₂. The composition of composite is identified by EDS linked to HRTEM (as shown in Fig. 3 d), which indicates that composite is composed of Ti, O and Ag elements.

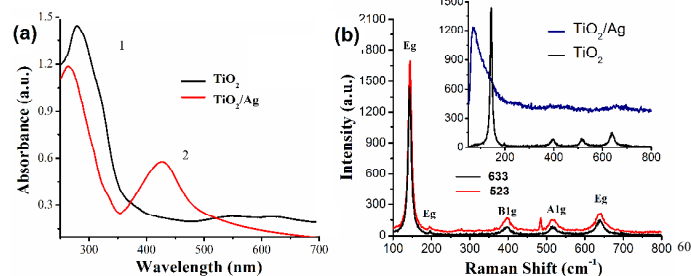


Fig. 4 (a) UV-Visible absorption spectrum of as-prepared TiO₂ and TiO₂/Ag FSMPs; (b) Raman spectra of as-prepared TiO₂ FSMP under 523 and 633 nm excitation sources, and the inset is Raman spectra of TiO₂ and TiO₂/Ag FSMPs under a 633 excitation source.

Fig. 4a shows UV-Visible absorption spectra of as-prepared TiO₂ and TiO₂/Ag FSMPs, respectively. Curve 1 shows one representative peak at about 295 nm, which is assigned to the

characteristic absorption peak of TiO₂ FSMPs. Compared with TiO₂ FSMPs, a representative peak at 425 nm is observed, which is caused by the excitation of surface plasmon vibrations of L-tyrosine reduced Ag NPs.²⁸ The powerful absorption of Ag SPR for TiO₂/Ag FSMPs indicates that the TiO₂/Ag FSMPs exhibit a good absorption in visible light region. It is noted that the characteristic absorption of TiO₂ is shifted to lower wavelength for the TiO₂/Ag composite, which is due to the change of the particles size and surrounding materials by introducing Ag NP.²⁹ Fig. 4b shows the Raman spectra of as-prepared TiO₂ FSMPs. Five representative Raman peaks are observed at 143.32 cm⁻¹, 196.98 cm⁻¹, 397.63 cm⁻¹, 515.44 cm⁻¹ and 639.09 cm⁻¹, respectively. Three representative Raman peaks at about 143.32 cm⁻¹, 196.98 cm⁻¹ and 639.09 cm⁻¹ are attributed to the Eg Raman active modes of anatase TiO₂ structures. Raman peaks at about 397.63 cm⁻¹ is attributed to the B1g Raman active mode of anatase TiO₂ structures. Raman peaks at about 515.44 cm⁻¹ is attributed to the A1g Raman active mode of anatase TiO₂ structures. Compared with the Raman spectrum under a 633 nm excitation source, a new peak of 485 nm is observed in the Raman spectrum for the 523 nm excitation source due to higher excitation source.³¹ These results also indicate that the anatase TiO₂ structure is fabricated via the method. The inset of Fig. 4 b shows the Raman spectra of TiO₂ and TiO₂/Ag FSMPs under a 633 excitation source. There is a blue shifted of peak from 144 to 75 nm for TiO₂/Ag FSMPs due to the incorporation of Ag NPs.

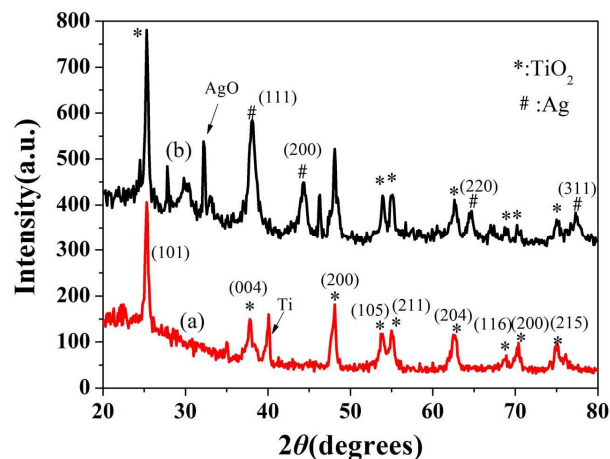


Fig. 5 XRD patterns of as-prepared TiO₂ and TiO₂/Ag FSMPs.

The XRD pattern of as-prepared TiO₂ FSMPs is shown in Fig. 5 (curve a). Nine major characteristic diffraction peaks are observed. The position of the characteristic peak (40.2°) is ascribed to (1 0 1) plane of Titanium (JCPDS, No.44-1294). The positions of the characteristic diffraction peaks (25.3°, 37.8°, 48.1°, 53.9°, 55.1°, 62.7°, 68.9°, 70.4°, 75°) are correspond to (101), (004), (200), (105), (211), (204), (116), (200) and (215) lattice planes of TiO₂ (JCPDS, No. 21-1272), respectively.³² The overwhelmingly intensive diffraction located at 2θ (25.3°) correspond to the (1 0 1) lattice plane of anatase crystal TiO₂

nanoparticles, which shows that the anatase crystal TiO₂ FSMPs is fabricated. The typical XRD pattern of as-prepared TiO₂/Ag FSMPs is shown in Fig. 4 (curve b). Compared with as-prepared TiO₂ FSMPs, the positions of the characteristic diffraction peaks (37.9°, 44.1°, 64.2°, 77.3°) are ascribed to (111), (200), (220) and (311) planes of Ag (JCPDS, No.04-0783), respectively.³³ It is noted that the surface of Ag NP can be oxidized to AgO after as-prepared samples are placed for a period of time, which is confirmed by characteristic peak (32.2°) due to the (-111) plane of silver oxide (JCPDS, No.43-1038).

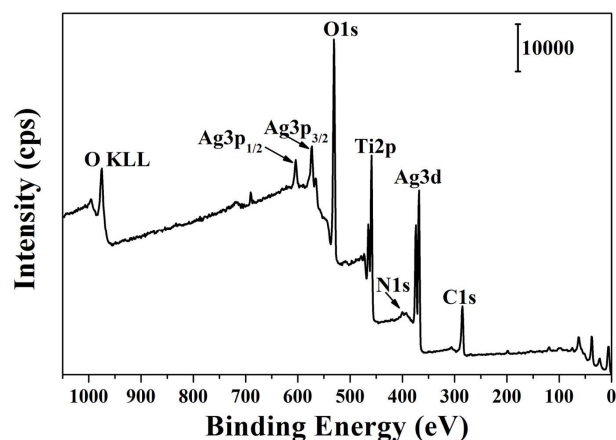


Fig. 6 XPS survey spectrum of the TiO₂/Ag FSMPs.

Although EDS spectrum and XRD analysis have effectively confirmed the existence of Ag and TiO₂, but these cannot distinguish the chemical states of the elements and explain the formation mechanism of the TiO₂/Ag FSMPs. So, XPS measurement is used to examine the valence states of Ag and Ti species in the TiO₂/Ag FSMPs and the formation mechanism of composites. The survey spectrum of the TiO₂/Ag FSMPs shows the presence peaks of C1s (BE = 285.33 eV), Ag3d (BE = 368.26 eV), N1s (BE = 400.08 eV), Ti2p (BE = 459.11 eV), and O1s (BE = 530.84 eV) (as shown in Fig. 6). The appearance of N1s peak at 400.08 eV in XPS survey spectrum is attributed to the nitrogen atoms present in amine groups of L-tyrosine.

As shown in Fig. 7a, the Ag3d core-level spectrum with two peaks at binding energies of 367.88 eV and 373.88 eV, corresponding to the Ag3d_{5/2} and Ag3d_{3/2} peaks, respectively. The gap of 6.0 eV between the two peaks is also indicative of metallic Ag⁰. There is no evidence for the presence of Ag⁺, indicating that the Ag ions in the composites are fully reduced to metallic Ag. However, the surface of as-prepared Ag nanoparticles will be oxidized to AgO after the as-prepared sample is placed for a period of time (as shown in the results of XRD). As shown in Fig. 7b, the Ti2p XPS spectrum with two peaks at binding energies of 458.88 and 464.58 eV, corresponding to the Ti2p_{3/2} and Ti2p_{1/2} peaks, respectively. These two peaks are attributed to the Ti⁴⁺ oxidation state, and the gap of 5.7 eV between the two peaks is also consistent with the Ti⁴⁺ oxidation state.³⁵ Fig. 7c shows the O1s core-level spectrum with two peaks located at binding

energies of 530.08 and 532.18 eV. The high binding energy of 530.08 eV can be attributed to Ti–O in TiO₂ nanocomposites. Other binding energy of 532.18 eV can be attributed to the OH⁻ on the surface of TiO₂ and tyrosine-capped TiO₂. As shown in Fig. 7d, the C1s core-level spectrum recorded from the nanocomposites has three main chemically distinct components at 284.98, 286.08, and 288.88 eV. The high binding energy of 288.88 eV can be attributed to the carboxylate carbon from the silver-bound tyrosine molecules. The binding energy of 284.98 eV can be attributed to the carbon of tyrosine. The binding energy of 286.08 eV can be attributed to the carbon adjacent to the amine groups in tyrosine as well as the amine bound to the OH⁻ on the surface of TiO₂. The XPS results confirm the existence of the Ag, tyrosine and TiO₂ in the composites.

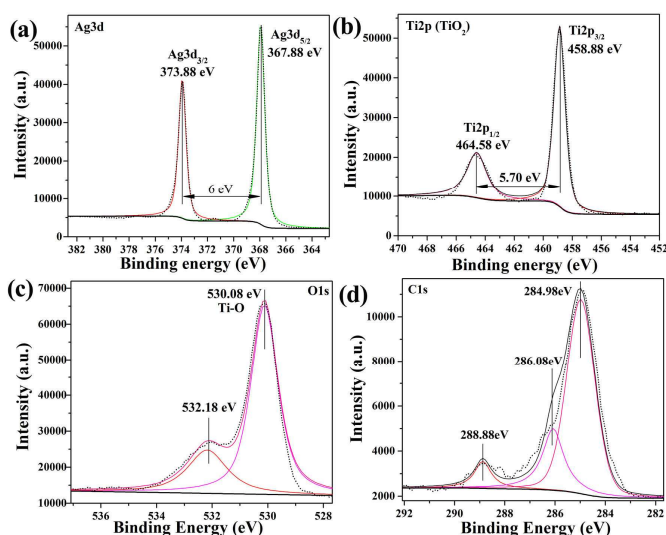


Fig. 7 XPS spectrum of the TiO₂/Ag FSMPs: (a) Ag3d, (b) Ti2p, (c) O1s and (d) C1s.

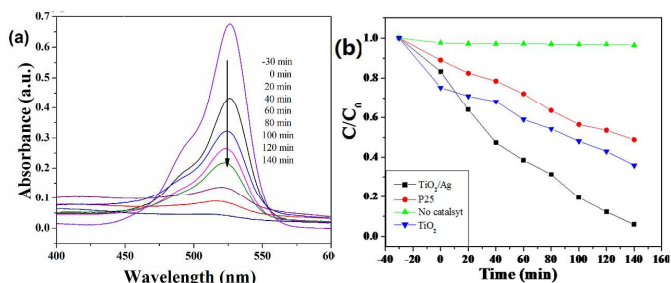


Fig. 8 (a) UV-vis absorbance of MB with different absorption times using TiO₂/Ag FSMPs; (b) photocatalytic degradation of the aqueous MB with as-prepared TiO₂ FSMPs, TiO₂/Ag FSMPs, and P25.

The dye MB is selected as the model molecules to evaluate the UV-light photocatalytic properties of as-prepared TiO₂ and TiO₂/Ag FSMPs. The P25 is also tested for comparison. The present photocatalytic tests are carried out in an aqueous solution containing oxygen (dissolved in the reaction system from air). In photocatalytic experiment, the degradation process is monitored by the change of the absorbance

maximum in optical absorption spectra of dyes. The UV-Vis absorption spectrum of MB using as-prepared TiO₂/Ag FSMPs with absorption time under UV-vis light radiation is shown in Fig. 8a, which shows that the MB content decreases with the increase of the light irradiation time.

The photocatalytic degradation of MB under UV-vis light radiation is used to evaluate the photocatalytic performance of as-prepared TiO₂ FSMPs, TiO₂/Ag FSMPs, and P25, as shown in Fig. 8b. Under dark condition, catalytic activity of TiO₂ FSMPs is higher than that of TiO₂/Ag FSMPs. That is because the surface area of composite (56.2 m²g⁻¹) is lower than that of TiO₂ FSMPs (63.5 m²g⁻¹) due to loading Ag NP. It is observed that the concentration of MB is hardly reduced under UV-visible light irradiation in the absence of the photocatalyst. The photocatalytic activity of TiO₂ FSMPs is higher than that of P25, which is attributed to a higher surface area of TiO₂ FSMPs (63.5 m²g⁻¹) than P25 (50 m²g⁻¹). However, the photocatalytic activity of TiO₂ FSMPs is further improved after loading Ag NPs. The photodegradation rate of the MB reaches to 77.5% for TiO₂/Ag FSMPs composites under light irradiation for 140 min. In the meantime, the photo-stability of TiO₂/Ag FSMPs by investigating its photocatalytic performance under light irradiation with three times of cycling uses is also studied. The results indicates the photodegradation rates are 77.5%, 76.2% and 74.3% for three times, respectively, which shows that the composite is stable under the studied conditions. The enhancement of the photocatalytic performance should be ascribed to the increase of the visible light absorption range and the reduction of electron-hole pair recombination in TiO₂ with the incorporation of Ag. Based on the experimental results, the higher photocatalytic activity of TiO₂/Ag FSMPs could be summarized as follows: (1) Higher surface area. Compared with P25, TiO₂/Ag FSMPs has a higher surface area. The higher surface areas result in the large contact areas between the active sites and the target substrate, which can increase the photocatalytic activity. (2) the reduction of electron-hole pair recombination. The work function position of Ag is lower than the conduction band position of TiO₂.^{36, 37} Therefore, under UV-light irradiation, such energy levels are beneficial for photo-induced electrons to transfer from the TiO₂ conduction band to Ag, which could efficiently separate the photo-induced electrons and hinder the charge recombination in electron-transfer processes, and thus enhance the photocatalytic performance. (3) Increase of visible light absorption. The strong absorption of visible light can be produced due to surface plasmon resonance (SPR) effect on the Ag NPs surface, which extends the spectral response of TiO₂/Ag FSMPs.^{38, 39}

4. Conclusions

In summarized, the novel TiO₂/Ag FSMPs were prepared for photocatalytic degradation of MB under light irradiation. The results show that the photocatalytic activities of TiO₂/Ag FSMPs are superior to that of as-prepared TiO₂ FSMPs and P25. The higher photocatalytic activity of TiO₂/Ag FSMPs can be attributed to higher surface area, increased light absorption capability, the reduction of electron-hole pair recombination.

Acknowledgments

This work is supported by the National Science Foundation of China (NSFC) (20871089, 21271136), the Scientific Research Found for Doctoral Program of Suzhou University (2014jyb07), the Important Project of Anhui Provincial Education Department (KJ2010ZD09), the Program of Innovative Research Team of Suzhou University (2013kytd02), and Outstanding Youth of Anhui Academy of Agricultural Sciences(13B1212)

Notes and references

¹Anhui Key Laboratory of Spin Electron and Nanomaterials, Suzhou University, Suzhou 234000, P. R. China, Tel.: +86-557-2871006; Fax: +86-557-2871003; E-mail: zhllisuzh@163.com; guang.zhu12@gmail.com
²Institute of Agro-products Processing, Anhui Academy of Agricultural Sciences, Hefei 230031, China

1. B. O. Regan and M. Graetze, *Nature*, 1991, **353**, 737.
2. T. Leshuk, R. Parviz, P. Everett, H. Krishnakumar, R. A. Varin, and F. Gu, *ACS Appl. Mater. Interfaces*, 2013, **5**, 1892.
3. X. J. Liu, X. J. Wang, H. L. Li, L. K. Pan, T. Lv, Z. Sun and C. Q. Sun, *J. Mater. Chem.*, 2012, **22**, 16293.
4. W. Yu, X. J. Liu, L. K. Pan, J. L. Li, J. Y. Liu, J. Zhang, P. Li, C. Chen and Z. Sun, *Appl. Surf. Sci.* 2014, **07**, 038.
5. X. J. Liu, L. K. Pan, T. Lv, T. Lu, Z. Sun and C. Q. Sun, *RSC Advances*, 2011, **1**, 1245.
6. Y. Wen, B. T. Liu, W. Zeng and Y. H. Wang, *Nanoscale*, 2013, **5**, 9739.
7. X. Chen and S. S. Mao, *Chem. Rev.*, 2007, **107**, 2891.
8. X. J. Liu, L. K. Pan, T. Lv and Z. Sun, *J. Alloy. Compd.*, 2014, **583**, 390.
9. B. Z. Tian, C. Z. Li, F. Gu and H. B. Jiang, *Catal. Commun.*, 2009, **10**, 925.
10. S. S. Zhang, F. Peng, H. J. Wang, H. Yu, S. Q. Zhang, J. Yang and H. J. Zhao, *Catal. Commun.*, 2011, **12**, 689.
11. M. Y. Xing, Y. M. Wu, J. L. Zhang and F. Chen, *Nanoscale*, 2010, **2**, 1233.
12. V. Iliev, D. Tomova, S. Rakovsky, A. Eliyas and G. L. Puma, *J. Mol. Catal. A: Chem.*, 2010, **327**, 51.
13. E. Kowalska, R. Abe and B. Ohtani, *Chem. Commun.*, 2009, **2**, 241.
14. Z. Xiong, J. Ma, W. J. Ng, T. D. Waite and X. S. Zhao, *Water Res.*, 2011, **45**, 2095.
15. M. V. Dozzi, L. Prati, P. Canton and E. Selli, *Phys. Chem. Chem. Phys.*, 2009, **11**, 7171.
16. X. D. Wang and R. A. Caruso, *J. Mater. Chem.*, 2011, **21**, 20.
17. Q. J. Xiang, J. Yu, B. Cheng and D. H. C. Ong, *Chem. Asian J.*, 2010, **5**, 1466.
18. J. Yu, G. Dai and B. Huang, *J. Phys. Chem. C*, 2009, **113**, 16394.
19. D. H. Yu, X. Yu, C. Wang, X. C. Liu and Y. Xing, *ACS Appl. Mater. Interfaces*, 2012, **4**, 2781.
20. J. Song, H. Kim, Y. Jang and J. Jang, *ACS Appl. Mater. Interfaces*, 2013, **5**, 11563.
21. T. Hirakawa, P. V. Kamat, *J. Am. Chem. Soc.*, 2005, **127**, 3928.
22. H. Zhang, C. Liang, J. Liu, Z. Tian, G. Wang and W. Cai, *Langmuir*, 2012, **28**, 3938.
23. W. Lu, G. Liu, S. Gao, S. Xing and J. Wang, *Nanotechnology*, 2008, **19**, 445711.
24. C. X. Wang, L. W. Yin, L. Y. Zhang, Y. X. Qi, N. Lun, and N. N. Liu, *Langmuir*, 2010, **26**, 12841.
25. P. R. Selvakannan, A. Swami, D. Srisathiyarayanan, P. S. Shirude, R. Pasricha, A. B. Mandale, and M. Sastry, *Langmuir*, 2004, **20**, 7825.
26. J. Du, J. Zhang, Z. Liu, B. Han, T. Jiang and Y. Huang, *Langmuir*, 2006, **22**, 1307.
27. X. F. Wu, H. Y. Song, J. M. Yoon, Y. T. Yu, and Y. F. Chen, *Langmuir*, 2009, **25**, 6438.
28. Z. Deng, M. Chen and L. Wu, *J. Phys. Chem. C*, 2007, **111**, 11692.
29. X. L. Hu, D. H. Li, Z. X. Shen, Q. H. Xiong, S. Z. Li, and H. J. Fan, *ACS Appl. Mater. Interfaces*, 2012, **4**, 2180.
30. T. C. Damato, C. C. S. Oliveira, R. A. Ando and P. H. Camargo, *Langmuir*, 2013, **29**, 1642.

31. Q. Guo, Z. C. Feng, G. N. Li, F. T. Fan, and C. Li, *J. Phys. Chem. C*, 2013, **117**, 2844.
33. G. Wu, J. Wang, D. F. Tomas, and A. Chen, *Langmuir*, 2008, **24**, 35053503.
- 5 33. B. Wang, L. Zhang, X. Zhou, *Spectrochim. Acta A.*, 2014, **121**, 63.
34. L. Zhang, C. Wang, Y. Zhang, *Appl. Surf. Sci.*, 2012, **258**, 5312.
35. J. K. Zhou, L. Lv, J. Yu, H. L. Li, P. Z. Guo, H. Sun and X. S. Zhao, *J. Phys. Chem. C*, 2008, **112**, 5316.
36. Y. M. Wu, H. B. Liu, J. L. Zhang and F. Chen, *J. Phys. Chem. C*,
10 2009, **113**, 14689.
37. G. Zhu, F. F. Su, T. Lv, L. K. Pan and Z. Sun, *Nanoscale Res. Lett.*, 2010, **5**, 1749.
38. X. Chen, Z. Zheng, X. Ke, E. Jaatinen, T. Xie, D. Wang, C. Guo, J. Zhao and H. Zhu, *Green Chem.*, 2010, **12**, 414.
- 15 39. S. Sun, W. Wang, L. Zhang, M. Shang and L. Wang, *Catal. Commun.*, 2009, **11**, 290.